Electronic supplementary information

Unveiling the Synergistic Effect of *A*-Site Doping in Perovskite Nanosheets and Electrode Modulation for Boosting Dielectric Performance of Printed Microcapacitors

Pengxiang Zhang [a], Binbin Zhang [a], Feng Dang [c], Ce-Wen Nan [d], and Bao-Wen Li [a, b, *]

[a] *State Key Laboratory of Silicate Materials for Architectures, School of Materials Science and Engineering, Wuhan University of Technology, Wuhan 430070, China*

[b] *State Key Laboratory of Advanced Technology for Materials Synthesis and Processing, Center of Smart Materials and Devices, Wuhan University of Technology, Wuhan 430070, China*

[c] *Key Laboratory for Liquid-Solid Structural Evolution and Processing of Materials (Ministry of Education), Shandong University, 17923 Jingshi Road, Jinan 250061, China*

[d] *State Key Lab of New Ceramics and Fine Processing, School of Materials Science and Engineering, Tsinghua University, Beijing, 100084, China*

*Corresponding Author:
E-mail address:
bwli@whut.edu.cn (B.-W. Li)

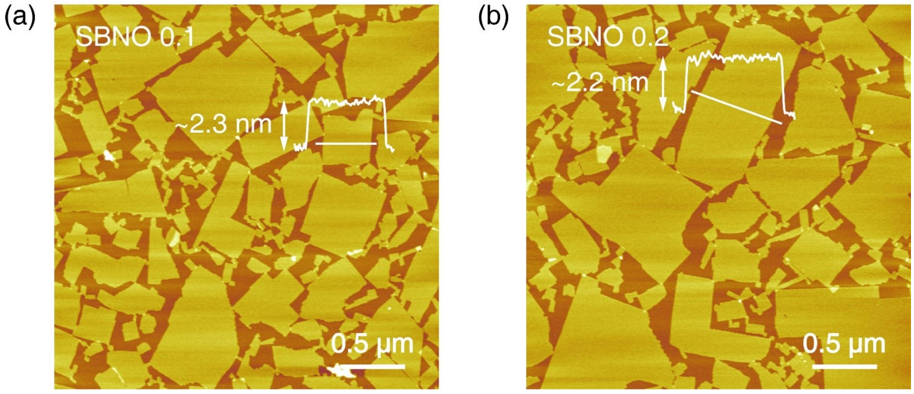

Figure S1. AFM images of (a) $Sr_{1.9}Bi_{0.1}Nb_3O_{10}$ and (b) $Sr_{1.8}Bi_{0.2}Nb_3O_{10}$ nanosheet, respectively. Inset: line profiles across individual nanosheet.

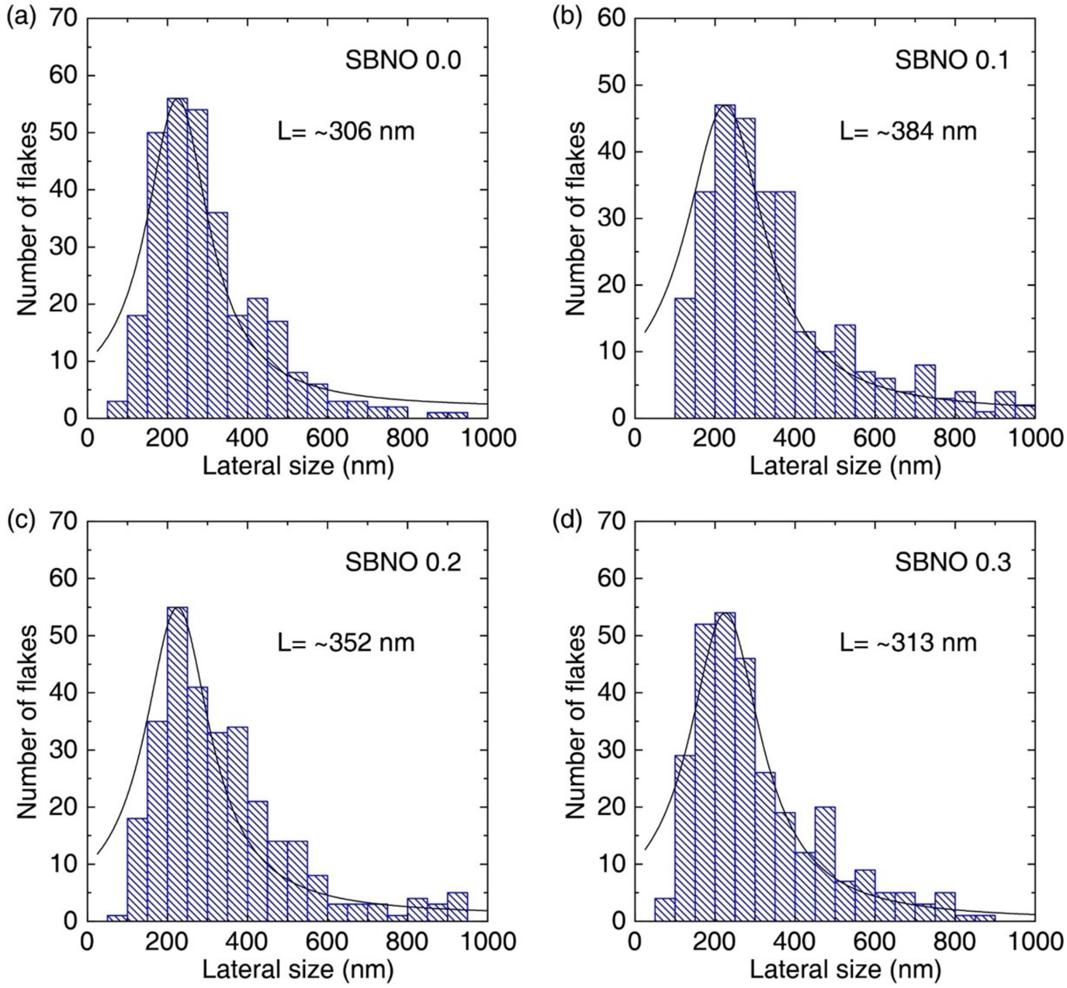

Figure S2. The lateral flake size distribution images of (a) $Sr_2Nb_3O_{10}$, (b) $Sr_{1.9}Bi_{0.1}Nb_3O_{10}$, (c) $Sr_{1.8}Bi_{0.2}Nb_3O_{10}$, and (d) $Sr_{1.7}Bi_{0.3}Nb_3O_{10}$ nanosheets.

Table S1. The rheological parameters including viscosity, surface tension, density, and *Z* value for $Sr_{2\text{-}x}Bi_xNb_3O_{10}$ (x = 0.0-0.3), graphene, and Ag ink.

	Viscosity (mPa·s)	Surface tension (mN/m)	Density (g/cm^3)	*Z* value
SBNO 0.0 ink	2.31	26.5	0.895	9.4
SBNO 0.1 ink	2.35	26.8	0.895	9.3
SBNO 0.2 ink	2.37	26.2	0.895	9.1
SBNO 0.3 ink	2.33	26.6	0.895	9.3
Gr ink	11.3	33	0.94	2.2
Ag ink	7.5	25	1.0	2.98

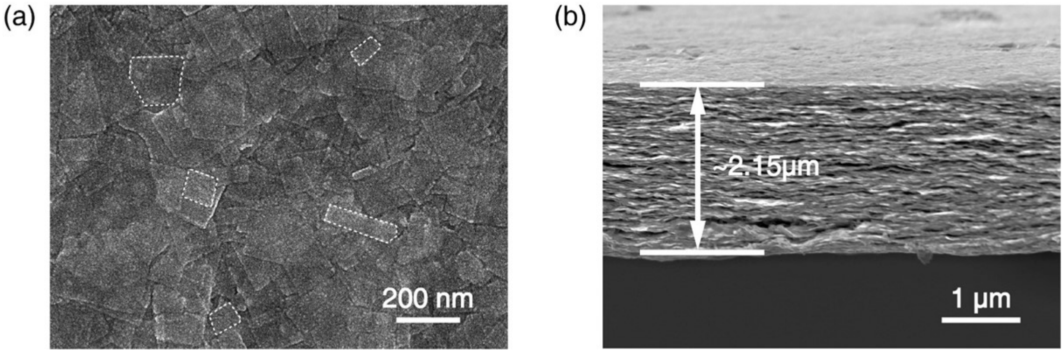

Figure S3. (a) Surface and (b) cross-sectional SEM images of inkjet-printed $Sr_{1.7}Bi_{0.3}Nb_3O_{10}$ films on a quartz glass substrate.

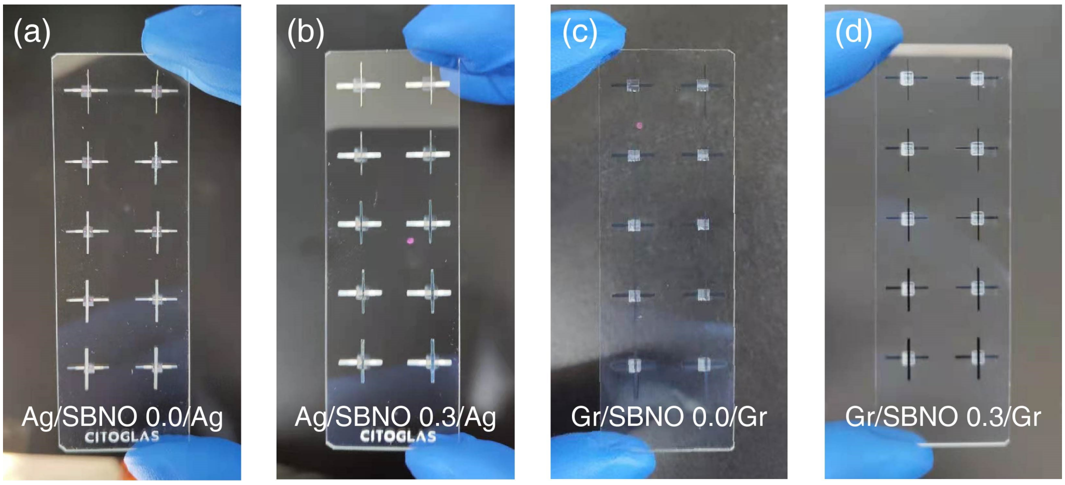

Figure S4. The optical photographs of inkjet-printed (a) Ag/SBNO 0.0/Ag, (b) Ag/SBNO 0.3/Ag, (c) Gr/SBNO 0.0/Gr, and (d) Gr/SBNO 0.3/Gr microcapacitors on a glass substrate.

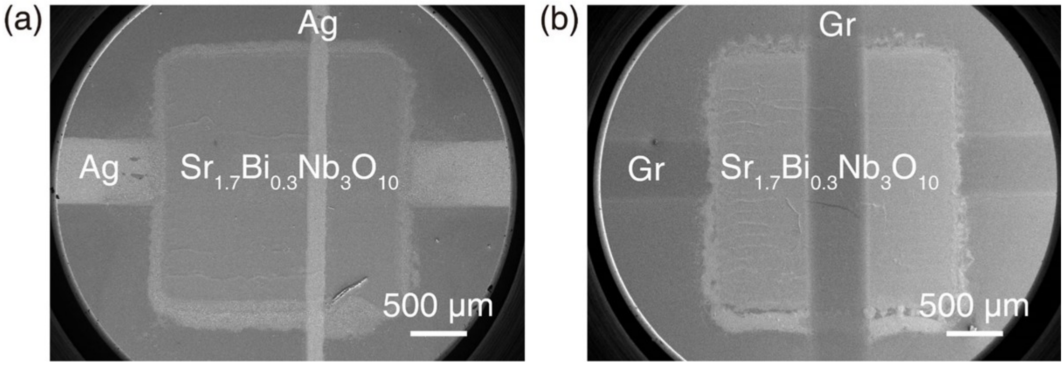

Figure. S5. SEM images of inkjet-printed Ag/SBNO 0.3/Ag and Gr/SBNO 0.3/Gr microcapacitors on a glass substrate.

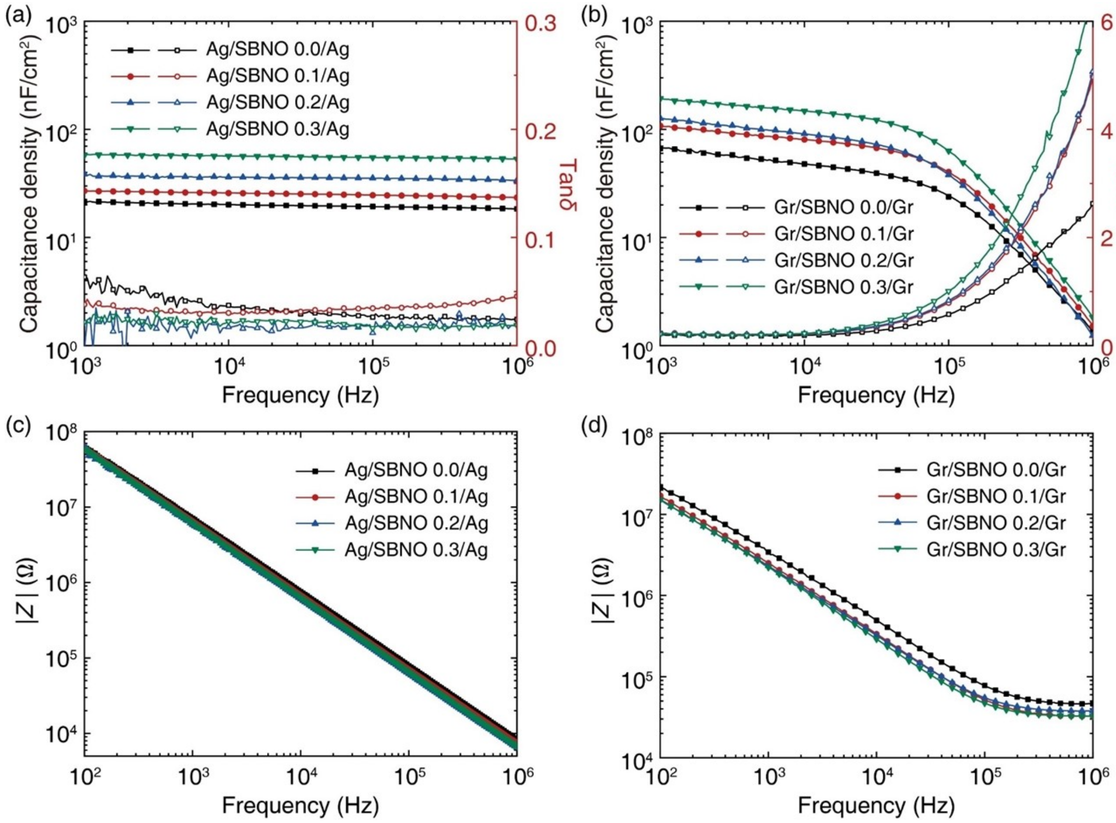

Figure S6. Frequency dependence of (a, b) capacitance density, tanδ and (c, d) impedance modulus values for inkjet-printed microcapacitors of (a, c) $Ag_B/Sr_{2-x}Bi_xNb_3O_{10}/Ag_T$ (x = 0.0-0.3) and (b, d) $Gr_B/Sr_{2-x}Bi_xNb_3O_{10}/Gr_T$ (x = 0.0-0.3), respectively.

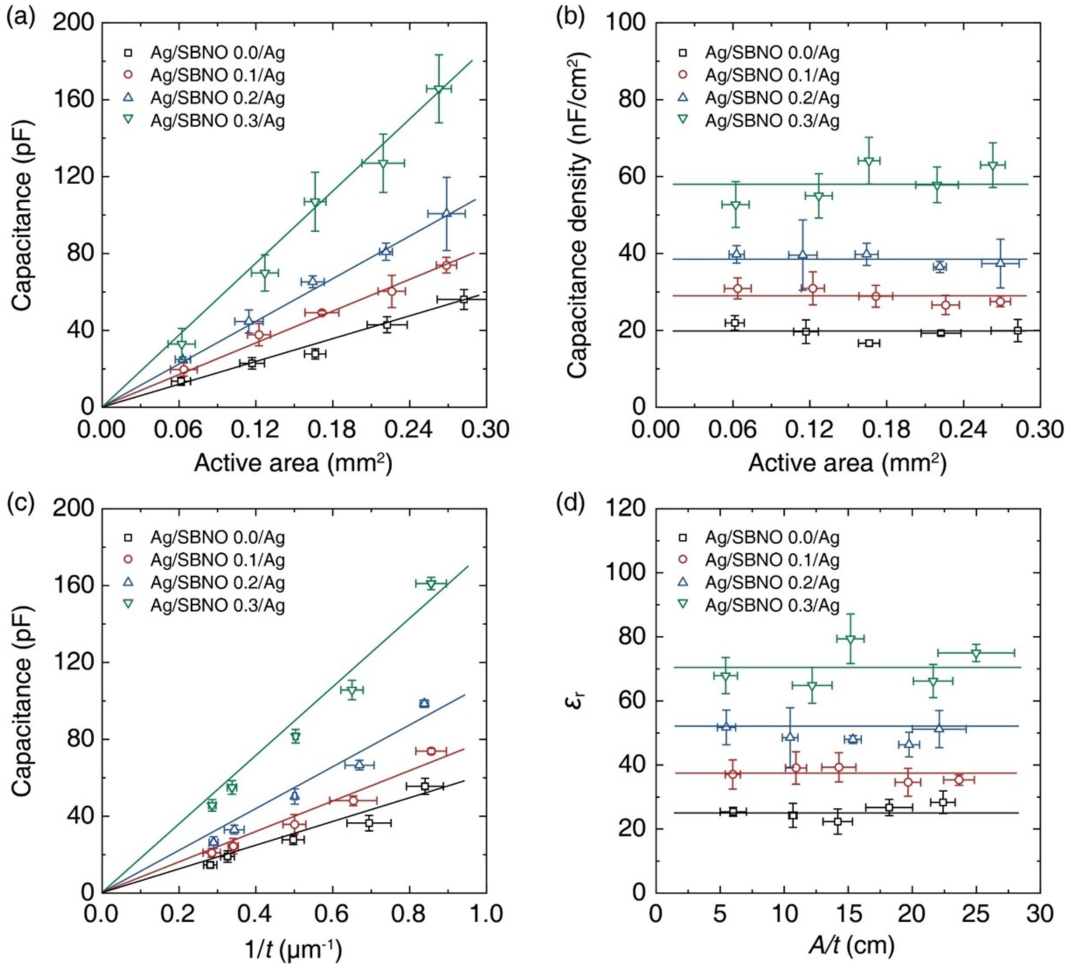

Figure S7. Dielectric performance of inkjet-printed $Ag_B/Sr_{2-x}Bi_xNb_3O_{10}/Ag_T$ (x = 0.0-0.3) microcapacitors. Active area dependence of (a) capacitance and (b) capacitance density for inkjet-printed microcapacitors with a dielectric-layer thickness (t) of ~1.2 µm. (c) The curve of capacitance as a function of reverse thickness for inkjet-printed microcapacitors with the active area (s) of ~0.25 mm^2. (d) The curve of relative permittivity as a function of the ratio of active area to thickness.

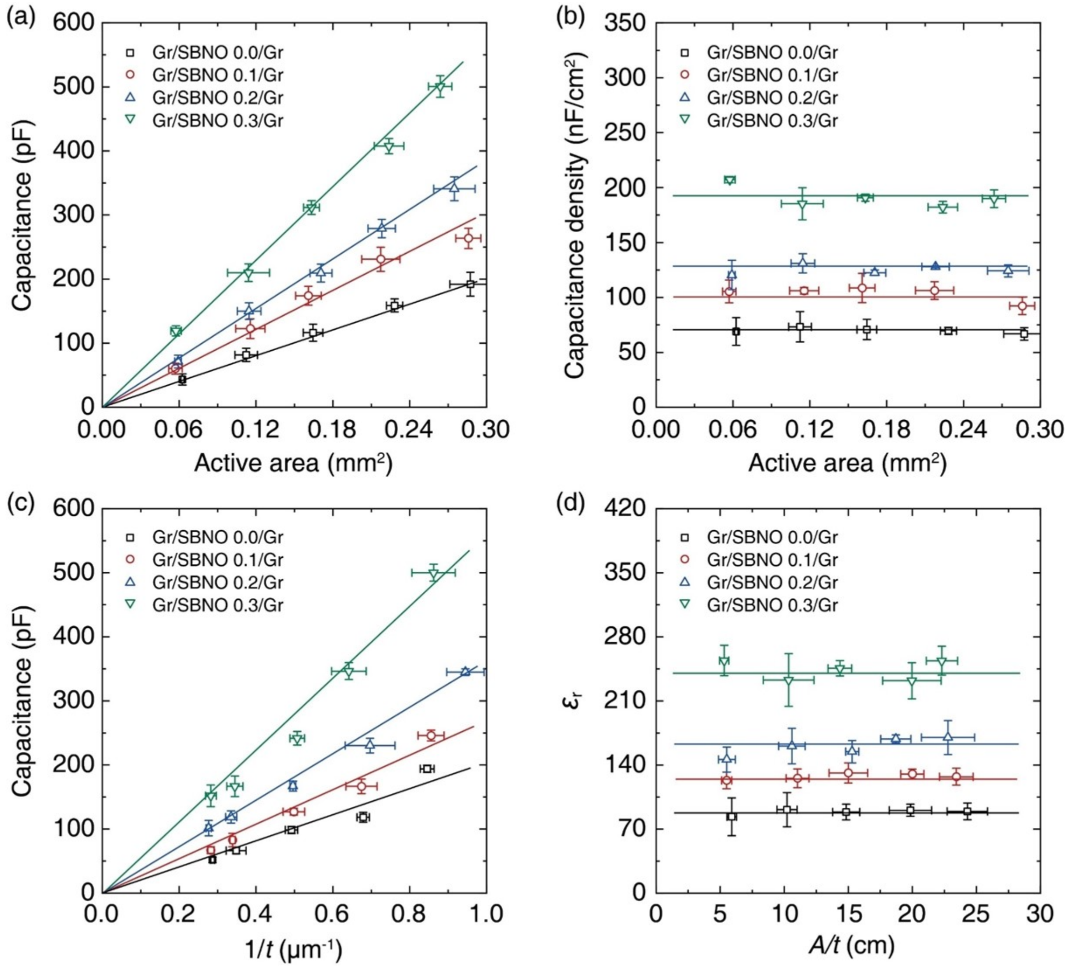

Figure S8. Dielectric performance of inkjet-printed $Gr_B/Sr_{2-x}Bi_xNb_3O_{10}/Gr_T$ (x = 0.0-0.3) microcapacitors. Active area dependence of (a) capacitance and (b) capacitance density for inkjet-printed microcapacitors with a dielectric-layer thickness (t) of ~1.2 μm. (c) The curve of capacitance as a function of reverse thickness for inkjet-printed microcapacitors with the active area (s) of ~0.25 mm^2. (d) The curve of relative permittivity as a function of the ratio of active area to thickness.

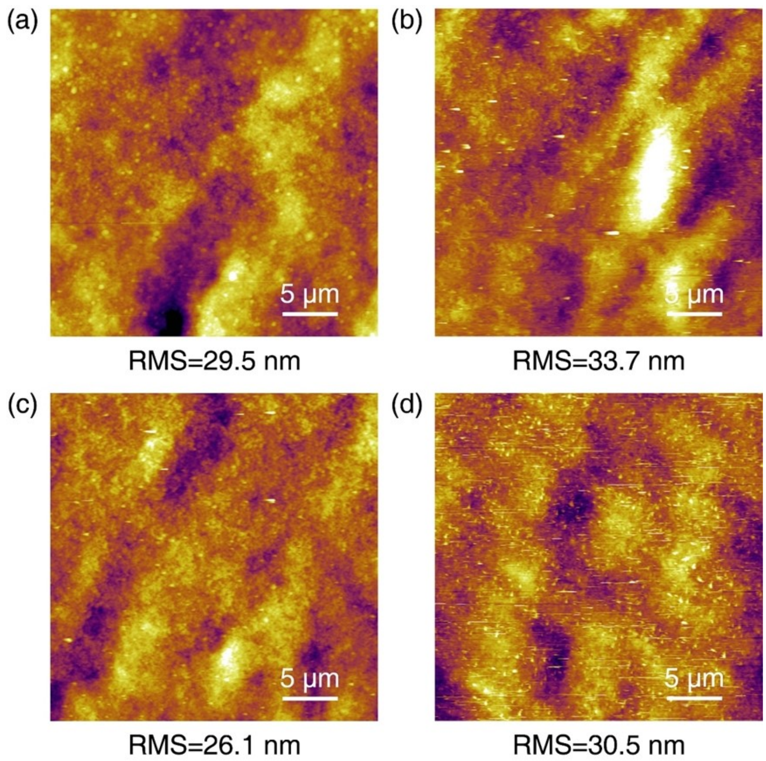

Figure S9. AFM images of inkjet-printed (a) $Ag_B/Sr_2Nb_3O_{10}/Ag_T$, (b) $Ag_B/Sr_{1.9}Bi_{0.1}Nb_3O_{10}/Ag_T$, (c) $Ag_B/Sr_{1.8}Bi_{0.2}Nb_3O_{10}/Ag_T$, and (d) $Ag_B/Sr_{1.7}Bi_{0.3}Nb_3O_{10}/Ag_T$ microcapacitors on a glass substrate.

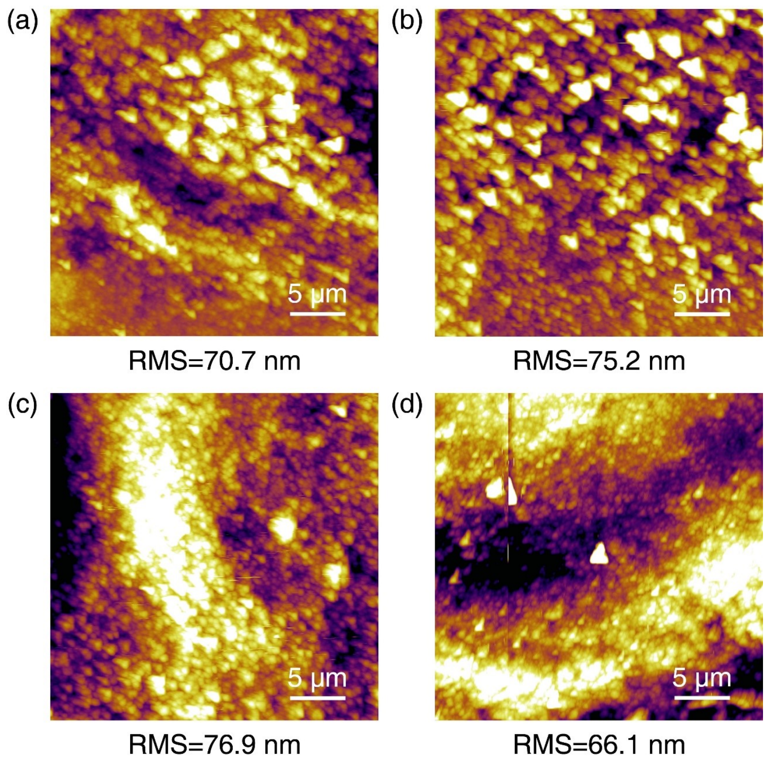

Figure S10. AFM images of inkjet-printed (a) $Gr_B/Sr_2Nb_3O_{10}/Gr_T$, (b) $Gr_B/Sr_{1.9}Bi_{0.1}Nb_3O_{10}/Gr_T$, (c) $Gr_B/Sr_{1.8}Bi_{0.2}Nb_3O_{10}/Gr_T$, and (d) $Gr_B/Sr_{1.7}Bi_{0.3}Nb_3O_{10}/Gr_T$ microcapacitors on a glass substrate.

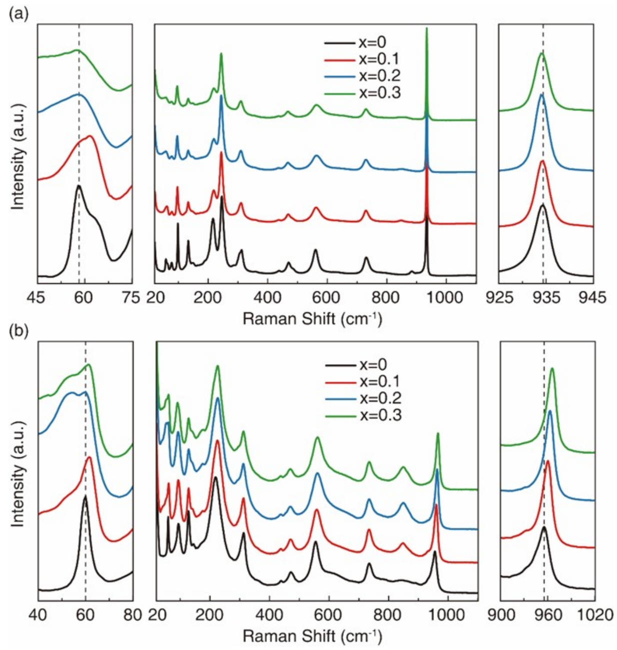

Figure S11. Raman spectra of (a) $KSr_{2\text{-}x}Bi_xNb_3O_{10}$ and (b) $HSr_{2\text{-}x}Bi_xNb_3O_{10}{\cdot}nH_2O$ (x = 0, 0.1, 0.2, and 0.3) powders.

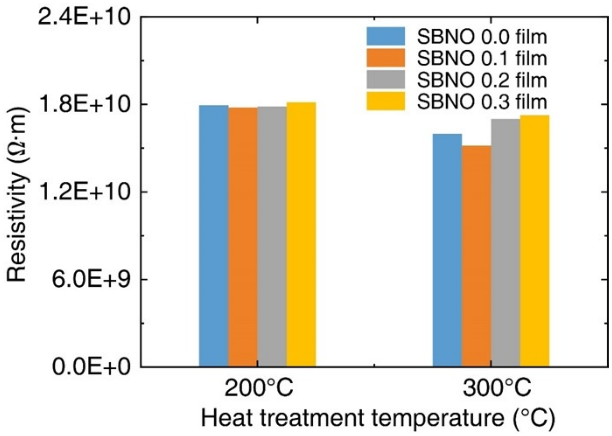

Figure S12. The surface resistivity of inkjet-printed $Sr_{2-x}Bi_xNb_3O_{10}$ (x = 0.0-0.3) film at different heat treatment temperatures.

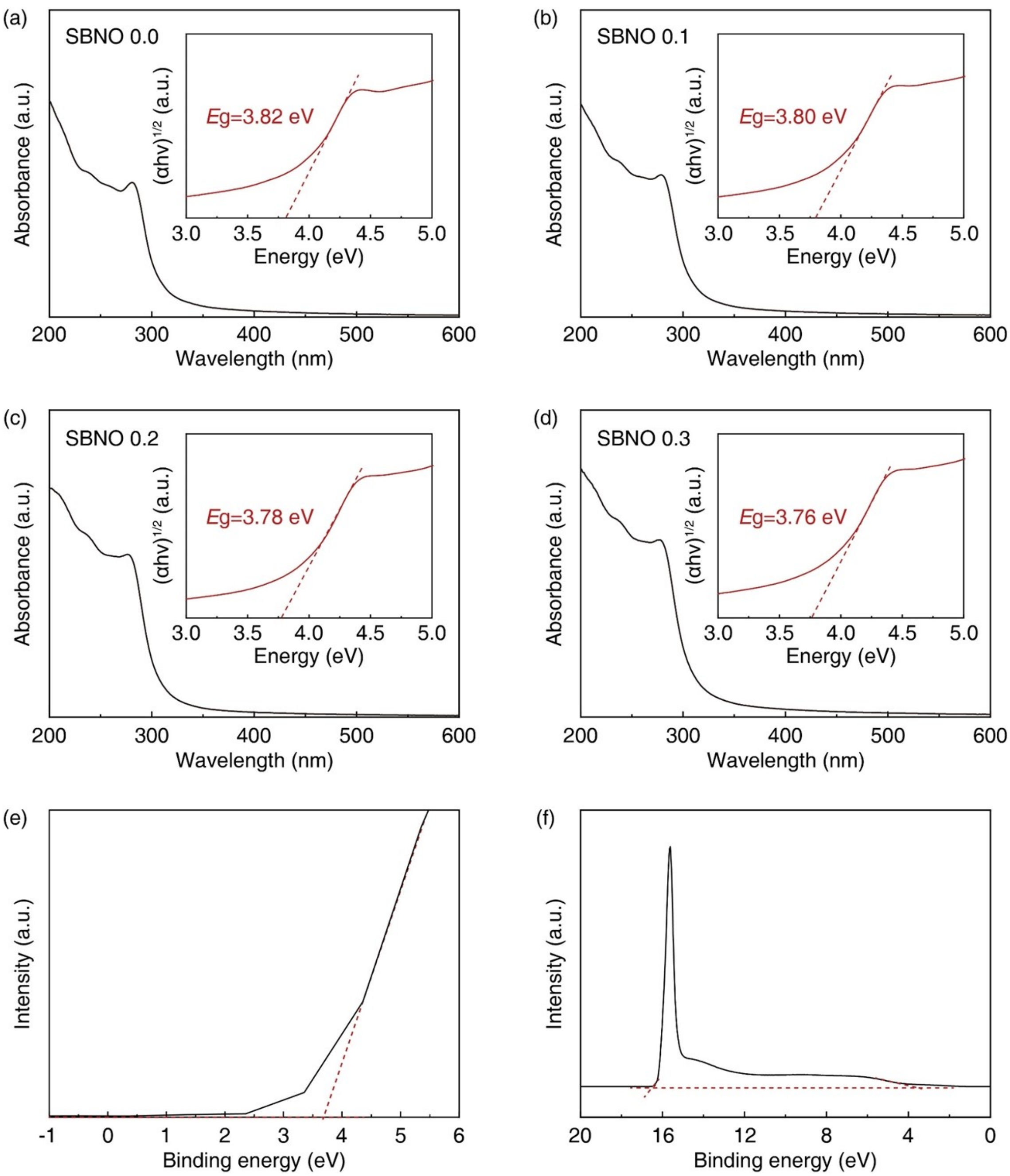

Figure S13. (a-d) UV-vis absorption spectra and the corresponding Tauc curve of $Sr_{2-x}Bi_xNb_3O_{10}$ (x = 0.0-0.3) film printed on the quartz substrate. (e) XPS valence bands and (f) UPS spectra as the estimation of work functions for $Sr_2Nb_3O_{10}$ film printed on the quartz substrate.

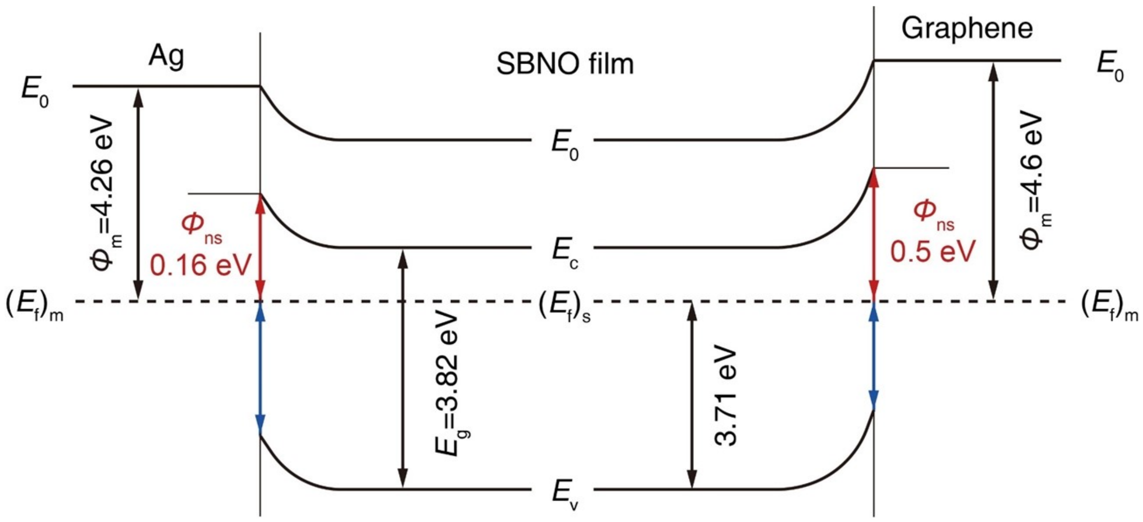

Figure S14. Energy band diagrams at the (a) Ag/$Sr_2Nb_3O_{10}$ film and (b) graphene/$Sr_2Nb_3O_{10}$ film interfaces, respectively.

Table S2. Lateral size statistics of $Sr_{2-x}Bi_xNb_3O_{10}$ (x = 0.0-0.3) perovskite nanosheets

Nanosheets	$Sr_2Nb_3O_{10}$	$Sr_{1.9}Bi_{0.1}Nb_3O_{10}$	$Sr_{1.8}Bi_{0.2}Nb_3O_{10}$	$Sr_{1.7}Bi_{0.3}Nb_3O_{10}$
Percentage of lateral size below 400 nm	78.3%	70.7%	72.3%	76.7%

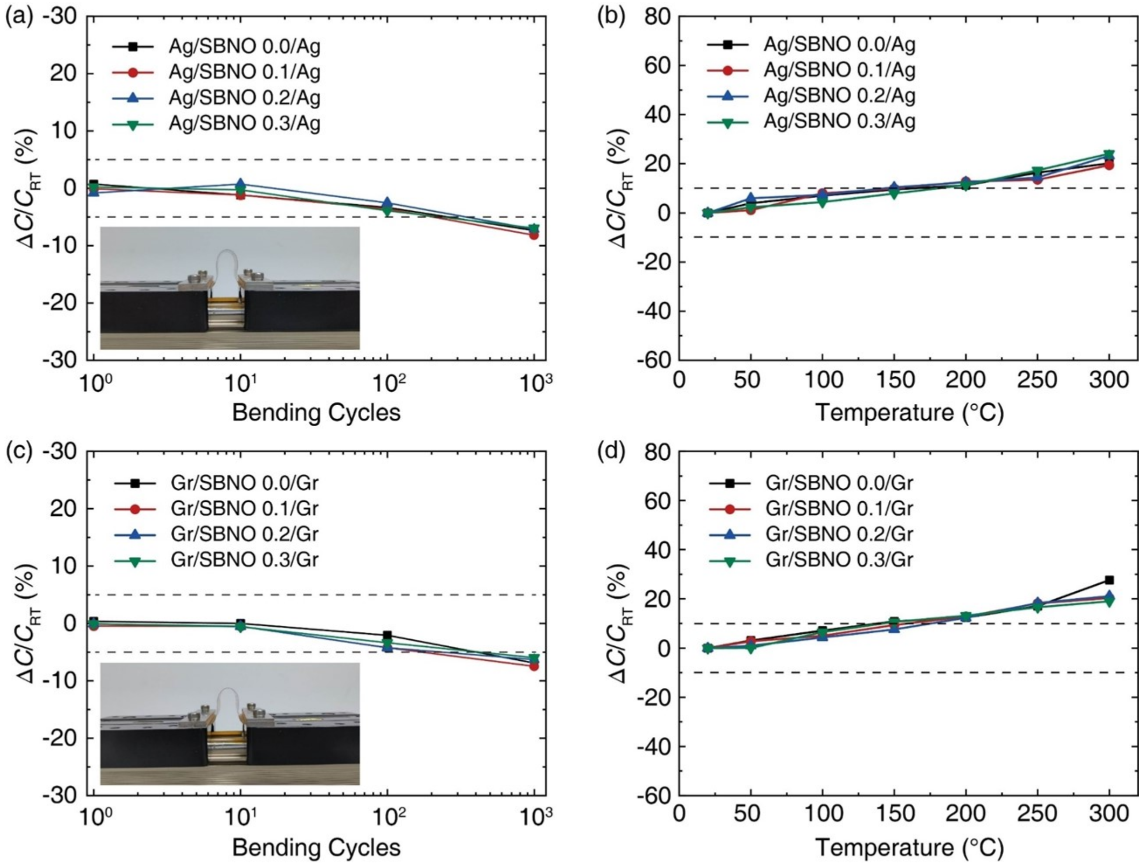

Figure S15. Electrical performance of inkjet-printed microcapacitors. Variation of capacitance as a function of bending cycles for inkjet-printed (a) $Ag_B/Sr_{2-x}Bi_xNb_3O_{10}/Ag_T$ (x = 0.0-0.3) and (c) $Gr_B/Sr_{2-x}Bi_xNb_3O_{10}/Gr_T$ (x = 0.0-0.3) microcapacitors, respectively. Variation of capacitance as a function of temperature for inkjet-printed (b) $Ag_B/Sr_{2-x}Bi_xNb_3O_{10}/Ag_T$ (x = 0.0-0.3) and (d) $Gr_B/Sr_{2-x}Bi_xNb_3O_{10}/Gr_T$ (x = 0.0-0.3) microcapacitors, respectively.

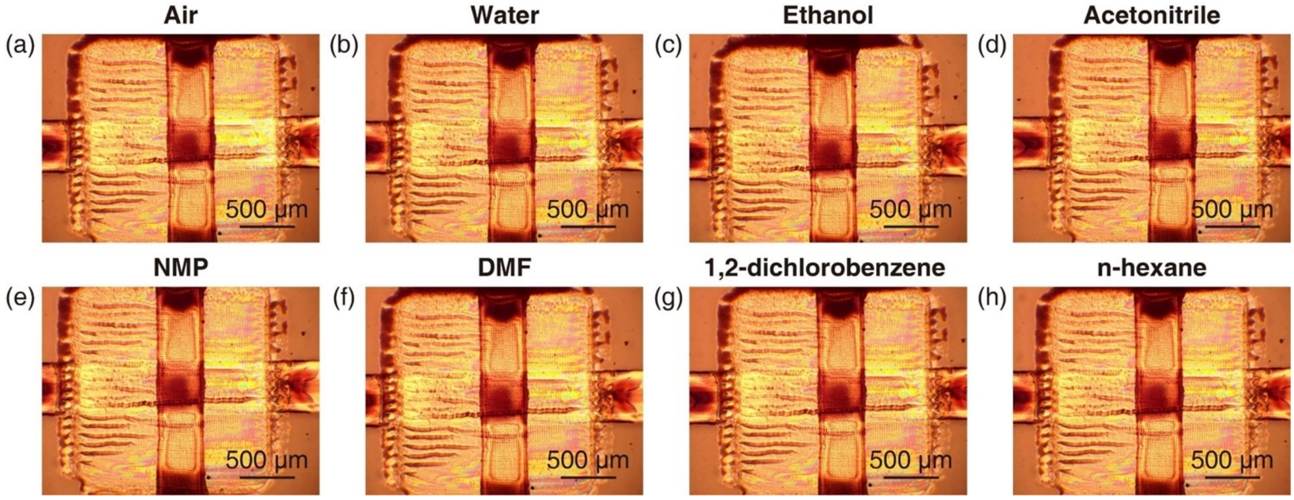

Figure S16. The optical photographs of $Ag_B/Sr_{1.7}Bi_{0.3}Nb_3O_{10}/Ag_T$ microcapacitors treated in (a) air, (b) water, (c) ethanol, (d) acetonitrile, (e) NMP, (f) DMF, (g) 1,2-dichlorobenzene, and (h) n-hexane.

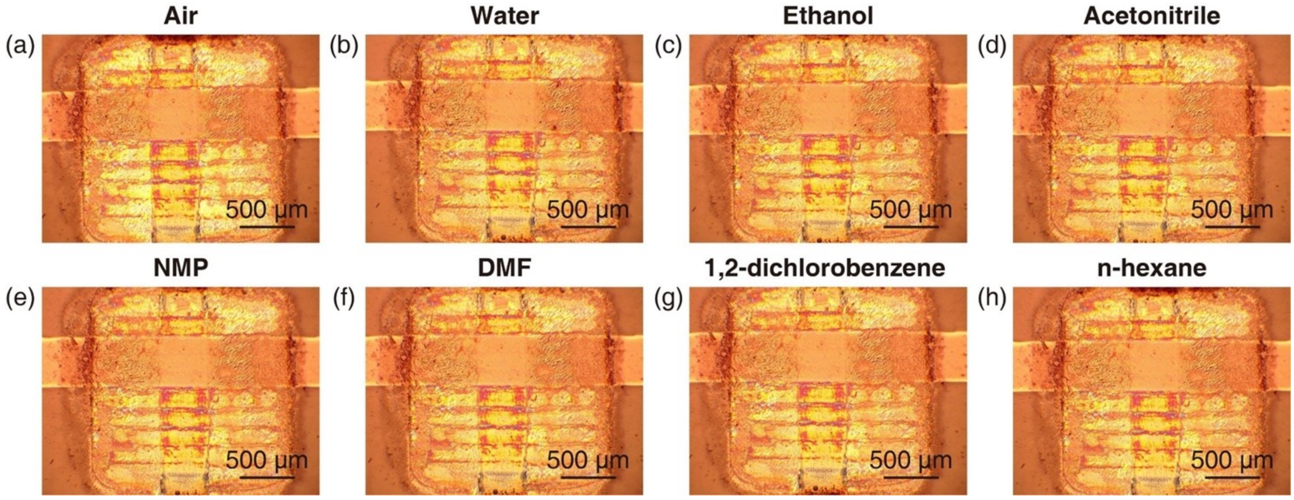

Figure S17. The optical photographs of $Gr_B/Sr_{1.7}Bi_{0.3}Nb_3O_{10}/Gr_T$ microcapacitors treated in (a) air, (b) water, (c) ethanol, (d) acetonitrile, (e) NMP, (f) DMF, (g) 1,2-dichlorobenzene, and (h) n-hexane.

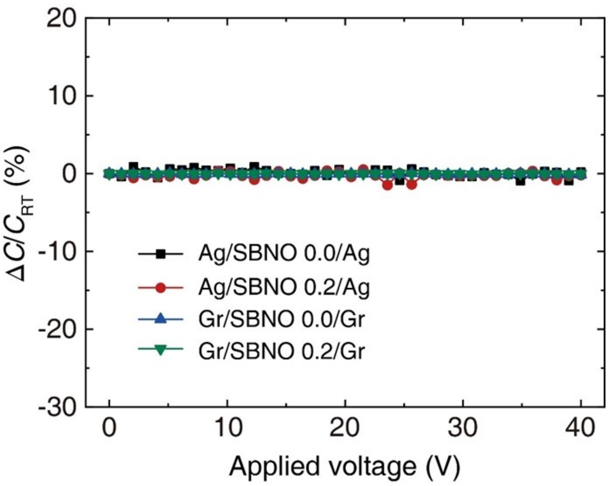

Figure S18. Electric field dependence of the capacitance variation for inkjet-printed $Ag_B/Sr_{2-x}Bi_xNb_3O_{10}/Ag_T$ (x = 0.0, 0.2) and $Gr_B/Sr_{2-x}Bi_xNb_3O_{10}/Gr_T$ (x = 0.0, 0.2) microcapacitors.

Table S3. Physical and chemical properties of different types of solvents[1-3].

Solvent	Polarity	Polarity index	Dielectric constant	Molecular weight (g/mol)
Water	Polar Protic	10.2	80.1	18.01524
Ethanol	Polar Protic	4.3	25.3	46.06844
Acetonitrile	Polar Aprotic	6.2	36.64	41.052
NMP	Polar Aprotic	6.7	32.55	99.13
DMF	Polar Aprotic	6.4	38.25	73.095
DCB	Non polar	2.7	9.32	147.01
Hexane	Non polar	0.06	1.89	86.175

Table S4. The yield and reproducibility of inkjet-printed microcapacitors.

Inkjet-printed microcapacitors	Sample quantity	Working	Yield and Reproducibility
$Ag/Sr_2Nb_3O_{10}/Ag$	15	12	80%
$Ag/Sr_{1.9}Bi_{0.1}Nb_3O_{10}/Ag$	15	14	93.3%
$Ag/Sr_{1.8}Bi_{0.2}Nb_3O_{10}/Ag$	15	13	86.7%
$Ag/Sr_{1.7}Bi_{0.3}Nb_3O_{10}/Ag$	15	13	86.7%
$Gr/Sr_2Nb_3O_{10}/Gr$	15	9	60%
$Gr/Sr_{1.9}Bi_{0.1}Nb_3O_{10}/Gr$	15	10	66.7%
$Gr/Sr_{1.8}Bi_{0.2}Nb_3O_{10}/Gr$	15	11	73.3%
$Gr/Sr_{1.7}Bi_{0.3}Nb_3O_{10}/Gr$	15	10	66.7%
Total	120	92	76.7%

References:

1. C. M. Hansen, *Hansen solubility parameters: a user's handbook*, CRC Press, 2007.
2. D. R. Lide, *CRC handbook of chemistry and physics*, CRC Press, 2004.
3. C. L. Yaws, *Thermophysical properties of chemicals and hydrocarbons*, William Andrew, 2008.